

# Electronic Delocalization, Vibrational Dynamics, and Energy Transfer in Organic Chromophores

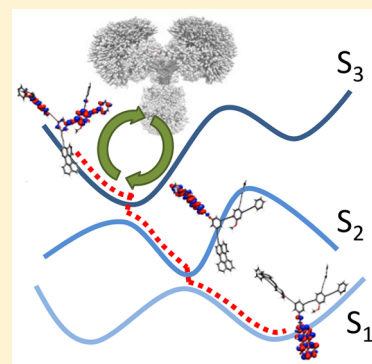
Tammie Nelson,<sup>†</sup> Sebastian Fernandez-Alberti,<sup>‡</sup> Adrian E. Roitberg,<sup>§</sup> and Sergei Tretiak<sup>\*,†</sup>

<sup>†</sup>Theoretical Division, Los Alamos National Laboratory, Los Alamos, New Mexico 87545, United States

<sup>‡</sup>Universidad Nacional de Quilmes/CONICET, Roque Saenz Peña 352, B1876BXD Bernal, Argentina

<sup>§</sup>Department of Chemistry, University of Florida, Gainesville, Florida 32611, United States

**ABSTRACT:** The efficiency of materials developed for solar energy and technological applications depends on the interplay between molecular architecture and light-induced electronic energy redistribution. The spatial localization of electronic excitations is very sensitive to molecular distortions. Vibrational nuclear motions can couple to electronic dynamics driving changes in localization. The electronic energy transfer among multiple chromophores arises from several distinct mechanisms that can give rise to experimentally measured signals. Atomistic simulations of coupled electron-vibrational dynamics can help uncover the nuclear motions directing energy flow. Through careful analysis of excited state wave function evolution and a useful fragmenting of multichromophore systems, through-bond transport and exciton hopping (through-space) mechanisms can be distinguished. Such insights are crucial in the interpretation of fluorescence anisotropy measurements and can aid materials design. This Perspective highlights the interconnected vibrational and electronic motions at the foundation of nonadiabatic dynamics where nuclear motions, including torsional rotations and bond vibrations, drive electronic transitions.



The efficient conversion of light energy into other usable forms of energy with minimal loss lies at the heart of our efforts to develop solar power as a clean energy source. Among natural organisms, the conversion of light energy, absorbed as solar radiation, into chemical energy is commonly achieved through highly efficient and complex arrays of conjugated chromophores.<sup>1,2</sup> The continuous development of new synthetic light harvesters that mimic natural photosynthetic complexes has produced a plethora of materials that can play the active role in organic photovoltaics, light emitting diodes, sensors, and a variety of other solar energy conversion applications. They range from supramolecular assemblies<sup>3</sup> and porphyrin- or bodipy-based chromophore arrays<sup>4–7</sup> and metal organic frameworks,<sup>8</sup> to macrocyclic polymers<sup>9,10</sup> and dendrimers<sup>11,12</sup> that combine several chromophores into a single giant molecule. A unifying theme among these synthetic light harvesting materials is the role of molecular architecture in determining the energy transfer dynamics that ultimately leads to energy transport and the spatial focusing of photon energy in the form of localized electronic excitations/excitons into target molecular systems. At the same time, molecular architecture can be exploited to minimize losses to heat (caused by vibrational relaxation) and losses of excitations (quenching) at defect sites. The key to designing new high efficiency materials is understanding the fundamental role of molecular architecture in guiding the electronic and vibrational dynamics and subsequent energy transfer processes.

Ideal light harvesting materials contain an inherent intramolecular energy gradient so that, following light absorption, an electronic excitation undergoes efficient and unidirectional

energy funneling to lower energy sites where emission or charge separation can occur. The efficiency of energy transfer is strongly tied to the associated time scale. Ultrafast energy transfer processes tend to be highly efficient because of the significant reduction in energy loss to other degrees of freedom, such as the solvent, that would be more probable for slower processes. Within this framework, the multichromophore systems mentioned above have emerged as promising candidates due to their  $\pi$ -conjugated structures composed of weakly coupled individual chromophore units. By incorporating multiple chromophores that absorb light at different wavelengths, the conversion efficiency can be enhanced. As a specific example highlighted in this Perspective, dendritic macromolecules combine several chromophores within a single well-defined and controllable molecular backbone. The wide range of dendritic structures are typically comprised of covalently linked chromophores where the backbone structure and conformation gives rise to built-in energy gradients and efficient intramolecular energy funneling.<sup>13,14</sup> The presence of multiple equivalent chromophore units in light-harvesting materials, including dendrimers, leads to a competition between intra- and inter-chromophore energy transfer pathways and introduces a complex interplay between electronic and vibrational transfer processes.

The movement of an excitation from one chromophore unit to another can be monitored by a variety of time-resolved

**Received:** April 1, 2017

**Accepted:** June 12, 2017

**Published:** June 12, 2017

77 spectroscopies, such as sophisticated 2D electronic spectroscopies<sup>15,16</sup> or conventional pump–probes.<sup>17,18</sup> For example, 79 changes in polarization can be detected through time-resolved 80 fluorescence anisotropy measurements. Such measurements 81 have been used to investigate excitation localization and 82 migration in natural<sup>19,20</sup> and artificial light harvesting systems 83 including nanorings,<sup>21</sup> macrocycles,<sup>9,10</sup> and dendrimers<sup>22</sup> as 84 well as conjugated polymers<sup>23,24</sup> and chromophore dimers.<sup>25,26</sup> 85 The electronic energy redistribution among chromophore units 86 induces a scrambling of the transition dipole orientation that 87 can occur through several possible mechanisms. First, a 88 delocalization of the electronic wave function can be induced 89 by strongly coupled chromophore units or by nuclear 90 relaxation. Alternatively, it is well-known that interactions 91 with molecular nuclear motions or the solvent environment in 92 conjugated polymers and dendrimers can result in changes to 93 optical properties and stabilization of spatially localized 94 excitations.<sup>27</sup> Similar sensitivity to the vibrational environment 95 has been observed in other materials such as nanodiamonds.<sup>28</sup> 96 For weakly coupled chromophores, a stochastic exciton 97 hopping mechanism can occur between sites localized in a 98 single unit. Exciton hopping is characterized by short-range 99 interchromophore energy migration between adjacent localized 100 sites (chromophores).<sup>29,30</sup> If geometric distortions are not 101 sufficient to bring electronic states into resonance, then exciton 102 hopping will be absent, and the complete relaxation can occur 103 within a single chromophore unit. In that case, localization 104 persists in a single unit where the choice of chromophore is 105 randomly distributed. Regardless of the mechanism, it is clear 106 that the vibrational dynamics and conformational disorder plays 107 a vital role in the energy transfer dynamics, and excitation 108 localization can be very sensitive to geometry distortions and 109 morphology changes.<sup>18,31–39</sup> The variation in the strength of 110 the nonadiabatic couplings, which modulate the interaction 111 between the electronic and vibrational degrees of freedom, and 112 the extent of exciton (de)localization both contribute to the 113 final electronic distribution among different chromophore units 114 following energy transfer.

Probing the formation, evolution, and decay of excitations in photoactive materials requires an understanding of nonadiabatic dynamics that couples electronic and nuclear motions.

115 Probing the formation, evolution, and decay of excitations in 116 photoactive materials requires an understanding of non- 117 adiabatic (NA) dynamics that couples electronic and nuclear 118 motions. NA dynamics can lead to energy transfer during the 119 nonradiative relaxation to the ground or low lying excited 120 states. The modeling of nanometer length scale and subnano- 121 second time scale dynamics of excited electron-vibrational 122 states can be achieved through mixed quantum-classical 123 dynamics methods to go beyond the Born–Oppenheimer 124 approximation. This Perspective is organized as follows: First, 125 we present a discussion of the methodology commonly used to 126 model NA dynamics in organic conjugated materials and the 127 analysis of electronic transition density matrices that can be 128 used to track changes in spatial localization resulting from 129 energy transfer. Next, we present examples of the effect of

conformational disorder and coupling of electronic and nuclear 130 motions on energy transfer dynamics. We demonstrate these 131 effects by analyzing nuclear motions in nanohoops, specifically 132 the torsional modes, that contribute to exciton trapping. 133 Finally, we consider the interpretation of energy transfer 134 mechanisms appearing in fluorescence depolarization. 135

*Nonadiabatic Excited-State Molecular Dynamics.* Modeling 136 dynamics on multiple coupled electronic states through regions 137 of strong nonadiabatic coupling can be performed using mixed 138 quantum classical trajectory surface hopping approaches.<sup>40</sup> 139 Generally, these methods rely on a classical treatment of nuclei 140 and a quantum mechanical description of electrons, which 141 evolve through the time-dependent Schrödinger equation 142 (TDSE) or Von Neumann equation with various prescriptions 143 for computing transition probabilities between coupled 144 electronic states. Numerous formulations of surface-hopping- 145 based simulations have been developed over the years to model 146 large molecular systems and can include decoherence effects 147 and spin–orbit coupling,<sup>41–50</sup> as well as quantum mechanics/ 148 molecular mechanics (QM/MM) methods for protein and 149 solution environments.<sup>51</sup> Popular among these methods is the 150 fewest switches surface hopping (FSSH) approach,<sup>52</sup> where 151 transitions between coupled electronic states describe the 152 feedback between the electronic system and nuclear motions, 153 and the probability of changing the active potential energy 154 surface (PES) is calculated based on the strength of the 155 nonadiabatic coupling. Energy transfer between states com- 156 monly takes place through the direction defined by the 157 nonadiabatic coupling vector (NACR), which is related to 158 specific excited state normal modes.<sup>53,54</sup> The direction of 159 NACR can be interpreted as the nonadiabatic contribution to 160 the direction of the main driving force on the nuclei during 161 electronic transitions, and the strength of the nonadiabatic 162 coupling can be strongly affected by the effective nuclear 163 velocities in the direction of the nonadiabatic coupling vector. 164 Furthermore, normal modes that actively participate in the 165 electronic relaxation processes are characterized by the highest 166 overlap with the nonadiabatic coupling vectors during the 167 electronic transitions, as demonstrated, for example, in 168 chlorophyll A,<sup>55</sup> confirming the relevance of the NACR 169 direction during energy transfer. 170

The nonadiabatic excited-state molecular dynamics (NA- 171 ESMD) methodology developed by our group incorporates 172 quantum transitions among excited states using the FSSH 173 scheme. Following photoexcitation, the electronic wavefunction 174 evolves through the TDSE, while nuclei evolve according to 175 Newton's equation or constant-temperature Langevin dynam- 176 ics<sup>56,57</sup> with forces from the excited state PES. The simulations 177 of coupled nuclear and electronic dynamics must use the true 178 PESs and forces in the excited states. This goes well beyond the 179 commonly used classical path approximation (CPA), where a 180 single trajectory and only the ground state PES is used. True 181 PESs are crucial for capturing the changes in forces between 182 electronic surfaces that promote localization/delocalization and 183 energy transfer. The collective electronic oscillator (CEO) 184 approach<sup>58,59</sup> is used to compute electronic excited states at the 185 configuration interaction singles (CIS) level of theory with a 186 semiempirical Hamiltonian.<sup>60,61</sup> Many independent trajectories 187 are required to generate a statistical ensemble where the 188 population of each quantum state is given by the fraction of 189 trajectories on each PES. Observables such as excited-state 190 lifetimes and energy transfer rates are averages over the 191 ensemble of trajectories, and the fluorescence anisotropy can be 192

193 directly modeled,<sup>62,63</sup> providing a level of mechanistic detail  
194 beyond what can be achieved through experiment alone. A  
195 detailed description of the NA-ESMD methodology can be  
196 found elsewhere.<sup>64–68</sup> These simulations have made it possible  
197 to successfully describe photoinduced processes in a variety of  
198 extended molecular systems.<sup>18,37,38,53,62,69–72</sup>

199 Implementation of hybrid quantum-classical methods, like  
200 FSSH, in extended conjugated molecules composed of sets of  
201 individual chromophores required a test of parameters and  
202 approximations previously proposed for model molecules.<sup>65</sup> It  
203 has been found that many previously suggested simplifications  
204 fail for realistic molecules with dense manifold of excited states,  
205 hundreds of vibrational degrees of freedom, and strongly  
206 varying vibrational frequencies and electron–phonon coupling  
207 constants.<sup>65,67</sup> For example, including NA couplings of states  
208 not directly involved in the internal conversion process can  
209 have a significant impact on the electronic relaxation rates.<sup>65</sup>  
210 Other simplifications that are not required in model systems,  
211 such as “on-the-fly” state limiting, have significantly reduced the  
212 computational costs for large systems.<sup>73</sup>

213 Additional considerations for modeling multichromophore  
214 molecules must be included in FSSH-based simulations to  
215 overcome its various limitations.<sup>43</sup> For spatially separated  
216 noninteracting electronic states brought into resonance by  
217 nuclear motions, we developed a state tracking algorithm<sup>66,74</sup> to  
218 distinguish between unavoided crossings involving interacting  
219 states (simulated by quantum hops) and trivial unavoided  
220 crossings between noninteracting states (detected by state  
221 tracking). Other solutions for the trivial crossing problem have  
222 been proposed.<sup>75–77</sup> In addition, several sophisticated  
223 approaches for incorporating decoherence in trajectory surface  
224 hopping simulations have also been developed over the  
225 years.<sup>44,77–80</sup> In recent years, there has been a renewed interest  
226 in deriving formally exact surface hopping approaches.<sup>81–83</sup> In  
227 particular, dynamical methods based on the propagation of  
228 Gaussian wavepackets, such as the widely used *ab initio*  
229 multiple spawning (AIMS) method<sup>84</sup> and others,<sup>42,85,86</sup> provide  
230 a fully *ab initio* description of quantum coherence effects.  
231 Despite their success, applications to large molecular systems  
232 (100s of atoms) are still typically too expensive. The NA-  
233 ESMD employs instantaneous decoherence<sup>67</sup> by resetting  
234 quantum amplitudes after a hop.

235 The NA-ESMD simulations presented in the following  
236 sections have been performed within the basis of adiabatic  
237 states. However, geometrical distortions can affect the energy  
238 ordering of the corresponding diabatic states, leading to a  
239 change in the electronic character and/or label of the adiabatic  
240 state. Therefore, it is more convenient to understand results in  
241 terms of diabatic states defined according to their electronic  
242 character. For clarity, we define the state labels used throughout  
243 the remainder of the discussion:  $S_n$  refers to the diabatic state  
244 where  $n$  refers to the initial energy ordering at time  $t = 0$ .

245 **Electronic Transition Densities.** The transition density (TD)  
246 matrices compactly reflect the properties of many-body wave  
247 functions and provide a simplified picture of wave function  
248 dynamics. Subsequently, these are convenient quantities to  
249 analyze energy transfer occurring through a change in the  
250 spatial excitation localization. Energy transfer and the extent of  
251 (de)localization can be followed in the NA-ESMD simulations  
252 through the spatial localization of the electronic TD. Transition  
253 density matrices are calculated within the CEO formalism<sup>58,59</sup>  
254 as  $(\rho^{0\alpha})_{nm} = \langle \phi_\alpha(r; \mathbf{R}(t)) | c_m^\dagger c_n | \phi_0(r; \mathbf{R}(t)) \rangle$  where  $\phi_0(r; \mathbf{R}(t))$  and  
255  $\phi_\alpha(r; \mathbf{R}(t))$  are the ground and excited state CIS adiabatic wave

functions, respectively.  $n$  and  $m$  represent atomic orbital (AO) 256  
basis functions, and  $c_m^\dagger$  and  $c_n$  are creation and annihilation 257  
operators. The diagonal elements  $(\rho^{0\alpha})_{mm}$  represent the net 258  
change in the electronic density distribution for a ground to 259  
excited state transition. In contrast, the off-diagonal elements of 260  
 $(\rho^{0\alpha})_{nm}$  describe electronic coherences and charge-transfer 261  
phenomena.<sup>87,88</sup> Subsequently, the orbital representation of 262  
these quantities is beneficial for the analysis of a variety of 263  
excited state properties. For example, natural transition orbitals 264  
(NTOs) developed by Martin<sup>89</sup> express the electronic 265  
transition density matrix as essential pairs of particle and hole 266  
orbitals, thus enabling examination of electron–hole separation 267  
in excitonic wave functions and charge-transfer states. 268  
Furthermore, the orbital representation of the diagonal 269  
elements is convenient to analyze the total spatial extent of 270  
the excited state wave function,<sup>68</sup> which is extensively used in 271  
this work. The normalization condition  $\sum_{n,m} (\rho^{0\alpha})_{nm}^2 = 1$  applies 272  
within the CIS approximation<sup>90</sup> owing to the fact that transition 273  
density matrices are normalized eigenvectors of the CIS 274  
operator. In multichromophore systems, it is convenient to 275  
partition the molecular system into chromophore fragments 276  
allowing the fraction of the transition density  $(\delta_X^\alpha)$  localized on 277  
each chromophore unit  $X$  to be found by summing the 278  
contributions from each atom (index  $A$ ) in  $X$  given by  $\delta_X^\alpha = 279$   
 $(\rho^{0\alpha})_X^2 = \sum_{n_A m_A} (\rho^{0\alpha})_{n_A m_A}^2$  280 p

While transition densities describe electronic systems, the evolution of vibrational degrees of freedom is reflected in nuclear motions.

*Analysis of Vibrational Dynamics.* While the transition 281  
densities describe the electronic system, the evolution of 282  
vibrational degrees of freedom is reflected in nuclear motions. 283  
Since it is impossible to follow all vibrational degrees of 284  
freedom, even for a small molecule, the nuclear motions that 285  
are strongly coupled to the electronic degrees of freedom serve 286  
as a convenient vibrational descriptor. In particular, bond 287  
length alternation (BLA) and torsions (dihedral angles) 288  
represent the fast and slow nuclear coordinates, respectively, 289  
common in soft conjugated organic materials.<sup>64,91</sup> The BLA 290  
gives the average difference between the single (C–C) and 291  
double (C=C) bond lengths of a vinylenic segment and is 292  
defined by  $[\{(d_1 + d_3)/2\} - d_2]$ , where  $d_1$  and  $d_3$  are the 293  
lengths of single bonds, and  $d_2$  is the length of the double bond. 294

*Conformational Disorder.* The ubiquitous soft molecular 295  
structure among organic conjugated polymers and chromo- 296  
phores leaves their molecular geometry highly susceptible to 297  
thermal fluctuations. These thermally induced geometry 298  
variations produce the effect commonly known as conforma- 299  
tional disorder. The conformational variation of the backbone 300  
geometry in organic conjugated materials, including den- 301  
drimers, impacts the electronic transition density localization 302  
and thus the relative balance between intra- and inter- 303  
chromophore energy transfer and the available through-space 304  
and sequential through-bond energy transfer mechanisms. The 305  
accessible space of the conformational landscape can be 306  
strongly influenced through thermal fluctuations and depends 307  
on steric interactions between units. The effect of conforma- 308

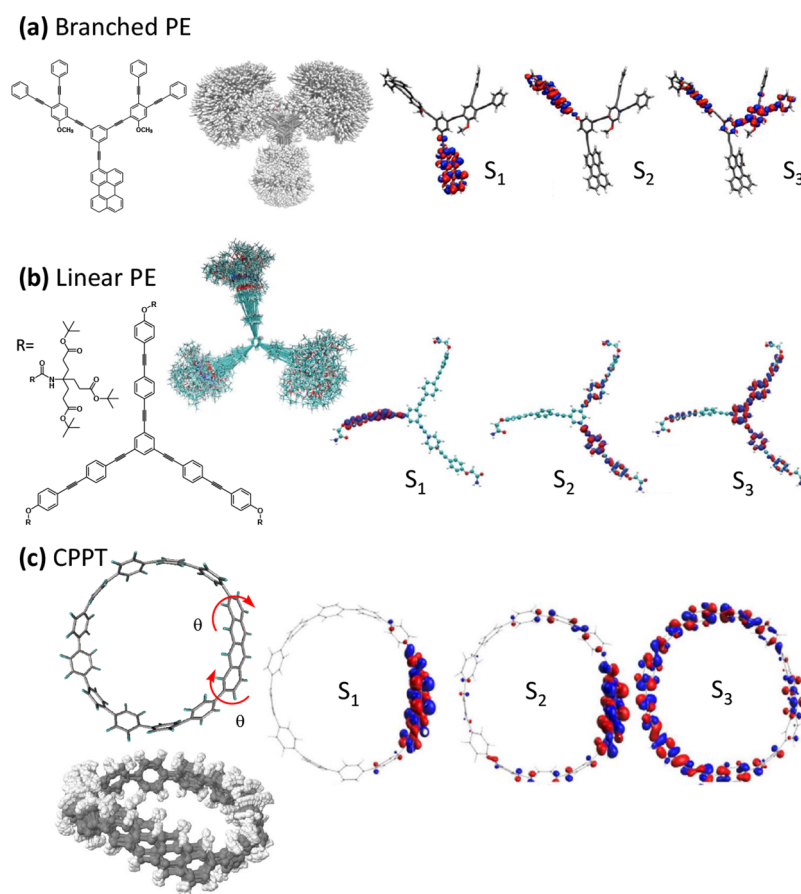


**Figure 1.** (a) Chemical structure of branched phenylene-ethynylene (PE) dendrimer and ground-state conformational disorder of 1000 configurations. The electronic transition density localization for the three lowest energy electronic excited states indicates energy funneling to a perylene sink in  $S_1$ . (b) Chemical structure of linear PE dendrimer and ground-state conformational disorder of 400 configurations. The electronic transition density localization for the three lowest energy electronic excited states suggest exciton trapping in a single branch in  $S_1$ . (c) Chemical structure of the nanohoop composed of cyclo para-phenylene with an inserted tetracene unit (CPPT) with large strain-induced dihedral angles around the tetracene defect and the resulting conformational disorder among 750 configurations. The electronic transition density localization for the three lowest energy electronic excited states indicates energy transfer to the tetracene insertion in  $S_1$ .

309 tional variation on the electronic TD localization is  
 310 demonstrated in Figure 1 for different molecular architectures.  
 311 The branched phenylene-ethynylene (PE) dendrimer<sup>18</sup> with  
 312 ortho, meta, and para linked units and an ethynylene-peryene  
 313 (EPer) energy sink shown in Figure 1a demonstrates  
 314 conformational disorder in the ground-state sampling of 1000  
 315 configurations. The orbital representation of the electronic TD  
 316 reveals an intramolecular energy gradient leading to fast energy  
 317 funneling to the sink. The changes in localization during  
 318 nonradiative relaxation leads to exciton trapping in the EPer  
 319 sink:  $S_{\geq 3}$  states are delocalized over both PE fragments, the  $S_2$   
 320 state is localized in one PE unit, and  $S_1$  is localized in the EPer  
 321 sink. Alternatively, the chemical structure of a PE dendrimer  
 322 with three equivalent linear PE units attached with meta  
 323 branching<sup>37</sup> in shown in Figure 1b. Dendrimers with  
 324 chromophores of the same conjugation length lack an energy  
 325 gradient. The superposition of molecular geometries obtained  
 326 from the ground-state QM/MM conformational sampling in  
 327 THF solvent reveals the conformational disorder. Despite the  
 328 absence of an energy gradient, the meta branching breaks the  
 329 conjugation leading to localized excitations: the transition  
 330 density of  $S_1$  is mostly localized in one PE branch, with  $S_2$  and  
 331  $S_3$  states delocalized between the two other branches. Finally,  
 332 we consider the chemical structure of the cyclo para-phenylene

(CPP) presented in Figure 1c. The nanohoop is composed of  
 333 10 phenyl units with an inserted tetracene defect (CPPT).<sup>70</sup>  
 334 The defect introduces strain in the hoop and large dihedral  
 335 angles produce geometric variations among the 750 depicted  
 336 ground-state configurations. In general, temperature-induced  
 337 conformational disorder in CPP systems leads to wider  
 338 torsional distributions, breaking the  $\pi$ -conjugation. This  
 339 symmetry breaking is more pronounced for large acenes  
 340 leading to state localization and exciton trapping. The  $S_1$  and  $S_2$   
 341 states of CPPT have TD strongly localized in the tetracene unit  
 342 while  $S_3$  is delocalized.  
 343

Conformational fluctuations can occur simultaneously with  
 344 electronic relaxation, making the energy transfer a dynamical  
 345 process rather than a static one.<sup>35</sup> Nuclear motions along a  
 346 dendrimer or polymer backbone can create quasi-degeneracy,  
 347 resulting in ultrafast changes to exciton localization, while, at  
 348 the same time, the electronic relaxation takes place between  
 349 states whose electronic character and localization are changing.  
 350 It is important to stress that energy transfer in systems  
 351 composed of chromophores of similar conjugation length can  
 352 rarely be described by a single well-defined pathway due to  
 353 conformational variety involving multiple chromophore  
 354 units.<sup>24,36</sup> In light harvesting complexes composed of multiple  
 355 chromophores, the energy transfer involves excitations 356

357 delocalized over multiple chromophores. As long as the donor  
 358 and acceptor sites are well separated in space, a rate description  
 359 based on Förster theory can be applied. However, conforma-  
 360 tional disorder can introduce kinks in the backbone of the  
 361 polymer to break the conjugation, which can significantly  
 362 impact the rate of excitation energy migration and electronic  
 363 relaxation. This has been experimentally confirmed, for  
 364 example, by photoluminescence anisotropy decay in PPV-  
 365 family conjugated polymers<sup>24</sup> and porphyrin nanorings.<sup>92</sup> As a  
 366 consequence, such kinks can lead to excited state energy  
 367 reordering and reverse directions of energy transfer,<sup>36</sup> overlap  
 368 between the absorbance of donor and acceptor units,  
 369 interference between multiple pathways,<sup>63</sup> and complex rates  
 370 that cannot be adequately described by a Förster model based  
 371 on a single rate.

Conformational disorder can introduce kinks in the backbone of the polymer to break the conjugation, which can significantly impact the rate of excitation energy migration and electronic relaxation.

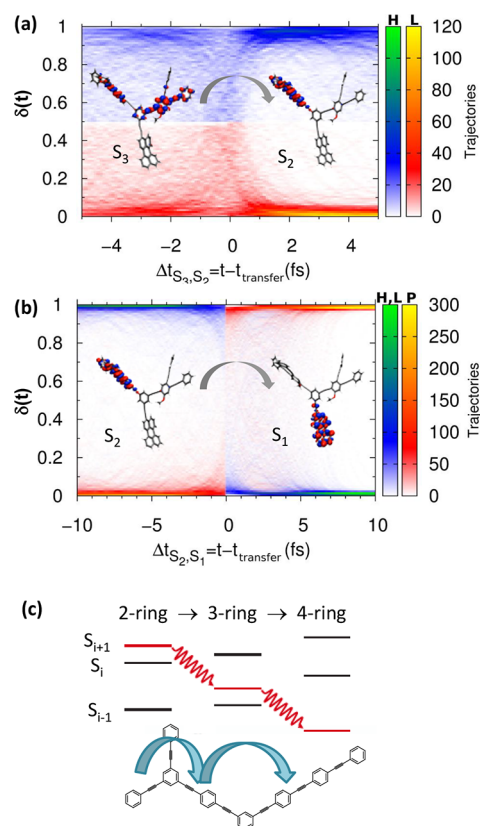


**Figure 2.** (a) Contour plot of the transition density composition before and after the  $S_3 \rightarrow S_2$  (delocalized PE state to localized PE state) transition. The blue-green color scale represents the PE unit with higher TD contribution (H) and the red-yellow color scale represents the PE unit with lower TD contribution (L). (b) Contour plot of the transition density composition before and after the  $S_2 \rightarrow S_1$  (localized PE state to localized trap state) transition. The blue-green color scale represents the PE units, while the red-yellow color scale represents the perylene trap (P). (c) Jablonski diagram depicting the unidirectional energy transfer mechanism that takes place due to differential nuclear motions in a model PE dendrimer.

372 *Electron-Vibrational Coupling Effects.* Let us consider more  
 373 closely the energy transfer in the branched PE dendrimer of  
 374 Figure 1a to demonstrate that changes in localization are  
 375 coupled to nuclear motions. Photoexcitation of the branched  
 376 PE dendrimer creates a delocalized excited state spanning both  
 377 PE units ( $S_{\geq 3}$ ) due to the high density of excited states (Frenkel  
 378 excitons) and the thermal fluctuations producing a variety of  
 379 initial conformations (see Figure 1a). During the nonradiative  
 380 relaxation, nonadiabatic transitions are driven by strong  
 381 coupling to high-frequency vibrational modes, causing the  
 382 excitation to quickly collapse to a more localized intermediate  
 383 state  $S_2$  in a single PE branch before finally reaching the EPer  
 384 sink in  $S_1$ .

385 Adiabatic vibrational relaxation of the lowest energy excited  
 386 state has been implicated in self-trapping of excitons through  
 387 strong coupling to torsional and C–C nuclear motions;  
 388 however, in this case, the localization occurs on an ultrafast  
 389 (subpicosecond) time scale. The change in the transition  
 390 density localization in the branched PE dendrimer around the  
 391  $S_3 \rightarrow S_2$  transition is revealed in the contour plot in Figure 2a.  
 392 The blue-green color scale indicates the transition density of  
 393 the PE unit with the higher TD contribution (labeled H), and  
 394 the red-yellow color scale corresponds to the other PE unit  
 395 with the lower contribution (labeled L). During the  $S_3 \rightarrow S_2$   
 396 transition, the electronic energy is located in the backbone with  
 397 negligible contribution from the EPer sink. The transition  
 398 occurs at  $\Delta t = 0$ . For  $\Delta t < 0$  the system is in the  $S_3$  state, and  
 399 the TD is delocalized over both PE units. After the transition, at  
 400  $\Delta t > 0$ , the system is in  $S_2$  and the contour distribution shows  
 401 the contribution of the L unit drops to almost 0, while most of  
 402 the TD is localized in the H unit, indicating that it becomes  
 403 localized on a single PE unit through coupling with the nuclear  
 404 dynamics. Similarly, the  $S_2 \rightarrow S_1$  transition corresponds to the  
 405 backbone-to-trap energy transfer, and the contour plot of the  
 406 transition density associated with this transition is shown in  
 407 Figure 2b. At the time of the nonadiabatic transition, the TD  
 408 changes from being localized in a single PE unit (blue) to being

fully localized in the EPer trap (red). This example highlights  
 the effect of electronic and vibrational coupling. The changes in  
 localization both within the PE branches and between the PE  
 units and the EPer trap are concomitant with the strong  
 nonadiabatic coupling represented by the  $S_3 \rightarrow S_2$  and  $S_2 \rightarrow S_1$   
 transitions, respectively. That is a clear indication that the  
 changes in localization are directly coupled to the nuclear  
 motions.

The coupling between vibrational motions and energy  
 transfer is clearly evident in the PE dendrimer shown in Figure  
 2c. In this system, energy transfer is induced by differential  
 nuclear motion on the PESs modulating the energy difference  
 between states and enforcing the unidirectional downhill  
 mechanism.<sup>69</sup> While the electronic population is mostly on  
 $S_{i+1}$  (localized in the 2-ring units), nuclear motions on the  $S_{i+1}$   
 surface keep the energy gap between  $S_{i+1}$  and  $S_i$  small. This  
 favors the energy transfer between them since the nonadiabatic  
 couplings are inversely proportional to the energy difference.<sup>93</sup>  
 After the electronic population is transferred to  $S_i$  (localized on  
 the 3-ring unit), the nuclear motion on  $S_i$  decouples  $S_i$  and  
 $S_{i+1}$  but starts to couple  $S_i$  with  $S_{i-1}$ . The energy transfer  
 between these new states persists until most of the population has  
 been transferred to  $S_{i-1}$  (localized in the 4-ring unit). It has been

432 demonstrated that the triple bond excitations coincide with the  
 433 localization of the electronic transition densities, meaning that  
 434 the energy transfer dynamics is a concerted electronic and  
 435 vibrational energy transfer process. This effect is captured in  
 436 simulation by using the “native” excited state forces which differ  
 437 on each surface and promote vibrational relaxation toward the  
 438 excited state energy minimum. The efficient energy funneling is  
 439 also observed in light harvesting donor–bridge–acceptor  
 440 systems.<sup>94,95</sup>

441 *Distinguishing Energy Transfer Mechanisms.* The redistribution  
 442 of transition density among equivalent chromophore units leads  
 443 to a scrambling of the transition dipole orientation. As  
 444 mentioned previously, for identical chromophore units, there  
 445 can be several mechanisms that can produce scrambling,  
 446 depending on how strongly chromophore units are coupled.  
 447 Strong coupling produces a true delocalization of the wave  
 448 function over multiple units. In the weak coupling regime, the  
 449 wave function maintains its localized nature in an individual  
 450 unit but either spatially migrates from unit to unit or relaxes  
 451 completely within a single unit where the choice of unit is  
 452 distributed among the identical chromophores.

For identical chromophore units,  
 there can be several mechanisms  
 that can produce scrambling,  
 depending on how strongly  
 chromophore units are coupled.

453 These mechanisms cannot always be distinguished from the  
 454 changes in the ensemble-averaged TD localization. For  
 455 instance, in the linear PE dendrimer composed of three  
 456 equivalent units, the initial excitation is broadly distributed  
 457 between two branches while the third branch is not excited.  
 458 The evolution of the ensemble-averaged transition density in  
 459 Figure 3a shows an equivalent final energy redistribution  
 460 among all three chromophore units. That distribution can be  
 461 achieved if all of the members of the ensemble have the  
 462 excitation delocalized over all three units or if excitations are  
 463 localized in a single branch with one-third of the ensemble  
 464 having the localization on the three different branches. In this  
 465 case, a close inspection of the transition density distributions is  
 466 required and reveals that the ensemble distribution has one-  
 467 third of the configurations with transition density localized in  
 468 any given unit, and the choice of the unit is randomly  
 469 distributed.

470 A similar result has been observed in dimers of organic  
 471 conjugated chromophores where both coherent wave-like  
 472 exciton motion and incoherent hopping mechanisms have  
 473 been observed in various dimer systems.<sup>26,96–98</sup> For example, in  
 474 dithia-anthracenophane (DTA), a sulfur connected dimer of  
 475 two identical anthracene units that localize excitations, previous  
 476 experimental and theoretical investigations supported a  
 477 coherent resonance energy transfer mechanism.<sup>25,99,100</sup> How-  
 478 ever, NA-ESMD simulations of DTA<sup>62</sup> revealed that the  
 479 ensemble-averaged TD exchange, shown in Figure 3(b), is due  
 480 to interchromophore exciton hopping between localized sites.  
 481 In this case, half of the trajectories finish completely localized  
 482 on one unit while the other half become fully localized on the  
 483 other unit. The initial nonadiabatic coupling between states  
 484 leads to an ultrafast exchange of energy between monomers  
 485 while thermally induced geometric distortions and vibrational

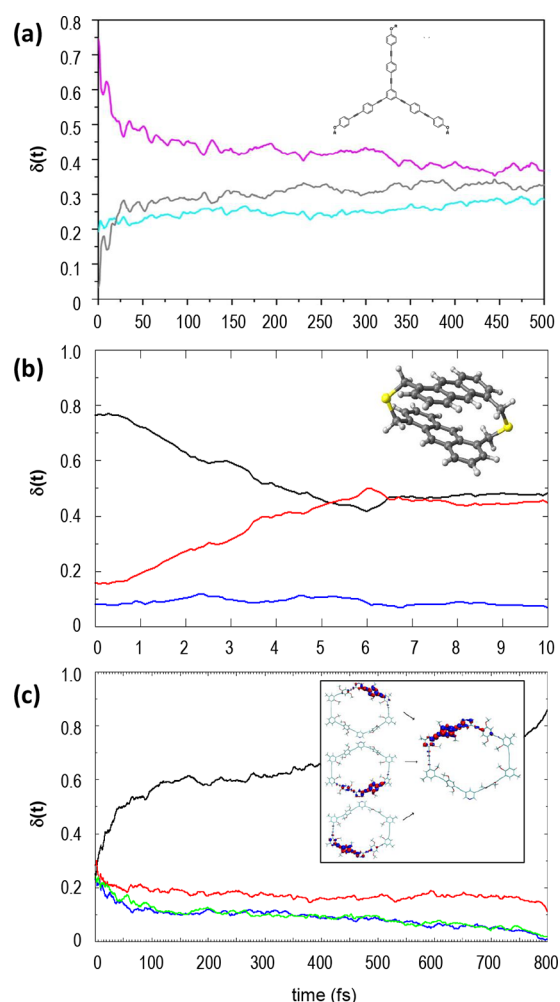


**Figure 3.** Evolution of the ensemble-averaged fraction of electronic transition density contained in individual chromophore units for (a) Three chromophore branches in the linear PE dendrimer, (b) two anthracene chromophores in a DTA dimer (red and black) and connecting sulfur atoms (blue), and (c) four chromophores in the PE macrocycle.

relaxation lead to localized electronic states. Ultimately, the  
 initial confinement of the spatial excitation due to energy  
 transfer during electronic relaxation is followed by interbranch  
 energy transfer, while the system remains in  $S_1$  corresponding  
 to hopping between localized transition densities.

Finally, we compare the result of the ensemble-averaged  
 transition density evolution in the linear PE dendrimer and  
 DTA bichromophore, which cannot be distinguished from a  
 true delocalization of the wave function, to the evolution in a  
 PE macrocycle having a final localization within a single  
 chromophore without subsequent changes in localization, just  
 as the linear PE dendrimer. However, unlike the previous  
 systems, Figure 3c shows an ensemble-averaged transition  
 density evolution in the macrocycle clearly revealing the rise in  
 localization within a single unit at the expense of the others.  
 The ambiguity is overcome in the macrocycle because of the  
 different choice of assignment used for tracking the units. In the  
 linear PE dendrimer and DTA, units are assigned based on the  
 initial localization of the electronic transition density. Based on  
 that assignment, one can clearly distinguish the loss of the  
 initially localized state, but the character of the final state is  
 ambiguous. Instead, the four units of the PE macrocycle are

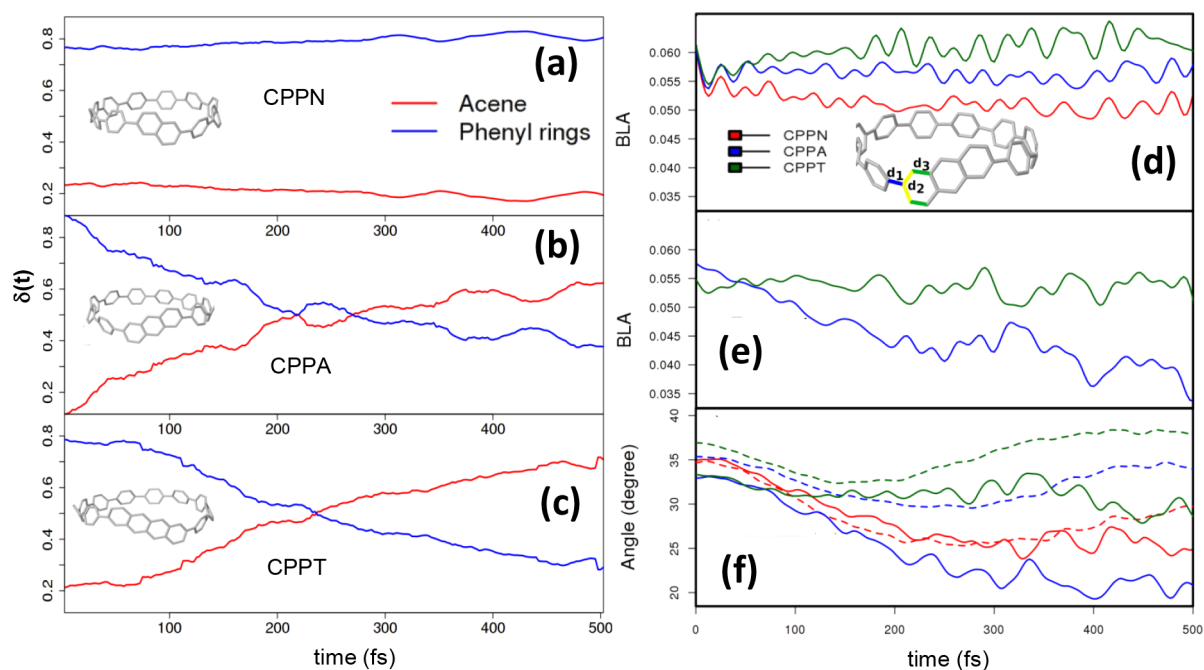


**Figure 4.** Time-dependent average fraction of transition density localized on the acene (red) and phenyl (blue) rings for (a) naphthalene (CPPN), (b) anthracene (CPPA), and (c) tetracene (CPPT). Evolution of the relevant vibrational motions for CPPN (red), CPPA (blue), and CPPT (green), including (d) the average bond length alternation (BLA) between phenyls, (e) the average BLA at the acene-phenylene junction, and (f) the average dihedral angles between phenyl rings (dashes) and at the acene-phenylene junction (solid).

508 assigned based on the *final* localization allowing the character  
509 of the final state to be distinguished.

510 The existence of multiple energy transfer pathways  
511 introduces another layer of complexity that can be solved  
512 using transition density flux methods<sup>63</sup> that allow the transition  
513 density exchange between specific units to be monitored. It is  
514 also possible to distinguish between inter- and intrachromo-  
515 phore relaxation channels by following the overlap between the  
516 current and final transition densities.<sup>38</sup>

517 *Strain-Induced Geometric Distortions.* Conjugated carbon  
518 nanohoops are an intriguing class of materials with unique  
519 optical properties<sup>101</sup> that combine strain, conformational  
520 disorder, and steric hindrance in unique ways that give rise to  
521 variations in the extent of conjugation within the molecular  
522 structure. These compounds have recently become popular  
523 candidates for light-harvesting applications and reveal a  
524 fascinating interplay between molecular distortions, delocaliza-  
525 tion and energy transfer.<sup>10,102–104</sup> For example, the redis-  
526 tribution of electronic energy in the acene-substituted CPPs<sup>70</sup> is  
527 strongly affected by the extent of geometric distortions  
528 introduced by the acene.

529 **Figure 4a–c** follows the changes in the electronic transition  
530 density localization in the phenyl rings and the acene unit for  
531 three different defect sizes: 2-rings (naphthalene), 3-rings  
532 (anthracene), and 4-rings (tetracene). Following excitation to  
533 an initially delocalized state spanning the phenyl rings, the  
534 excitation remains delocalized around the phenyl rings for the  
535 smallest acene substitution, naphthalene (CPPN; **Figure 4a**). In  
536 contrast, the excitation undergoes an ultrafast migration to the  
537 larger acenes. In anthracene (CPPA), the final transition  
538 density shown in **Figure 4b** is partially delocalized throughout  
539 the nanohoop and the anthracene. The energy transfer is most  
540 effective in tetracene (CPPT), as seen in **Figure 4c**, where the  
541 final excitation is concentrated on the tetracene unit. The larger

542 acenes introduce higher strain-induced geometric distortions  
543 that break the conjugation leading to localized states.

544 The torsions (dihedral angles) and bond-length alternations  
545 (BLAs), plotted in **Figure 4d–f**, represent relevant vibrational  
546 motions that receive electronic energy during the nonradiative  
547 relaxation.  $\pi$ -Conjugation tends to reduce the BLA values. The  
548 BLA between phenyl rings, **Figure 4d**, experiences an ultrafast  
549 reduction in all three systems, which persists for CPPN,  
550 reflecting the exciton delocalization that distorts the molecular  
551 geometry. In CPPT, the initial large ground-state BLA value is  
552 recovered, and CPPA experiences a partial recovery producing  
553 the partial exciton delocalization between the phenyl units and  
554 anthracene. The BLA at the acene-phenylene junction (**Figure**  
555 **4e**) undergoes a significant reduction for anthracene but not for  
556 tetracene, reflecting the larger extent of localization in  
557 tetracene. Smaller values of BLA at the anthracene-phenylene  
558 junction are associated with a higher degree of  $\pi$ -conjugation  
559 and exciton delocalization across the acene defect in CPPA. In  
560 CPPT, the large BLA value inhibits  $\pi$ -conjugation and leads to  
561 localization. The dihedral angles presented in **Figure 4f** for the  
562 acene-phenylene junction (solid) and phenyl-phenyl torsions  
563 (dashed) show a similar trend with the larger reduction moving  
564 from CPPT to CPPA to CPPN where the larger dihedral angles  
565 are associated with reduction of  $\pi$ -conjugation and stronger  
566 localization.

567 The substituted CPP nanohoops exemplify the connection  
568 between intramolecular exciton dynamics, energy transfer, and  
569 strain-induced nuclear motions in the electronic relaxation  
570 process. Similar connections have been observed in quantum  
571 dots where atomic fluctuations can lift degeneracy to overcome  
572 phonon bottlenecks in favor of fast relaxation.<sup>105</sup> Light  
573 harvesting within nanohoops is a complex process involving  
574 changes in localization controlled by intermediate electronic  
575 states and structural rearrangements, involving bond lengths

576 and torsion angles, that promote electronic energy redistrib-  
577 ution.

578 *Fluorescence Anisotropy.* The fluorescence anisotropy is often  
579 measured in experiment to detect changes in exciton  
580 localization during photodynamics by detecting changes in  
581 the transition dipole moment polarization caused by an  
582 excitation moving from one chromophore to another. The  
583 depolarization arises from the scrambling of the transition  
584 dipole orientation caused by either exciton hopping between  
585 equivalent sites or delocalization of the wave function among  
586 different units. The fluorescence anisotropy provides an  
587 important observable, allowing computational results to be  
588 directly connected with experimental measurement. In this  
589 case, the simulated fluorescence anisotropy can help decipher  
590 which mechanisms contribute to depolarization. The fluo-  
591 rescence anisotropy is calculated by the expression

$$C(t) = \frac{2}{5} \langle P_2(\vec{\mu}_A(0) \cdot \vec{\mu}_E(t)) \rangle$$

592 function of the absorption dipole moment of the chromophore  
593 at time zero,  $\vec{\mu}_A(t=0)$ , and its emission dipole moment at time  
594  $t$ ,  $\vec{\mu}_E(t)$ , where  $P_2(x) = \frac{1}{2}(3x^2 - 1)$  is the second-order  
595 Legendre polynomial,  $x$  is the cosine of the angle between  
596 the excitation and emission dipole moments, and the angular  
597 brackets indicate the average over all NA-ESMD trajectories.

Fluorescence anisotropy provides an important observable, allowing computational results to be directly connected with experimental measurement.

598 The final ensemble in linear PE corresponds to the random  
599 distribution of excitons trapped on different PE units, where  
600 there is a similar probability of each fragment retaining a  
601 significant contribution of the transition density. The spatial  
602 redistribution among the equivalent units results from the  
603 absence of an energy gradient. The experimental fluorescence  
604 anisotropy decay in the linear PE system observed in Figure 5a  
605 in black dots can be attributed to the confinement of the  
606 electronic wave function in a single branch and hopping  
607 between the branches rather than to its expansion over the  
608 whole dendrimer. In complexes that exhibit both relaxation  
609 within a single monomer unit and exciton hopping between  
610 localized units, the fluorescence depolarization is due to both  
611 the change in localization among different monomers and the  
612 changing emission dipole orientation within a single unit.  
613 Analyzing the fluorescence anisotropy signal from a single  
614 chromophore unit can reveal what extent of the depolarization  
615 arises from each mechanism. In the case of DTA, the simulated  
616 fluorescence anisotropy curves of the monomer dimethyl  
617 anthracene (DMA) and the DTA dimer are plotted in Figure  
618 5b. The curve for DMA represents the exciton relaxation  
619 confined to a single unit. Therefore, the additional depolariza-  
620 tion in DTA compared to DMA results from the change in  
621 localization associated with energy transfer between the rotated  
622 monomers. Similarly, Figure 5c shows the experimental and  
623 simulated depolarization curves for the PE macrocycle  
624 compared to the half ring. The macrocycle undergoes multiple  
625 energy transfer pathways from each unit to a single acceptor  
626 unit. Compared to the half ring, where energy transfer only  
627 occurs between two PE units, the additional depolarization in

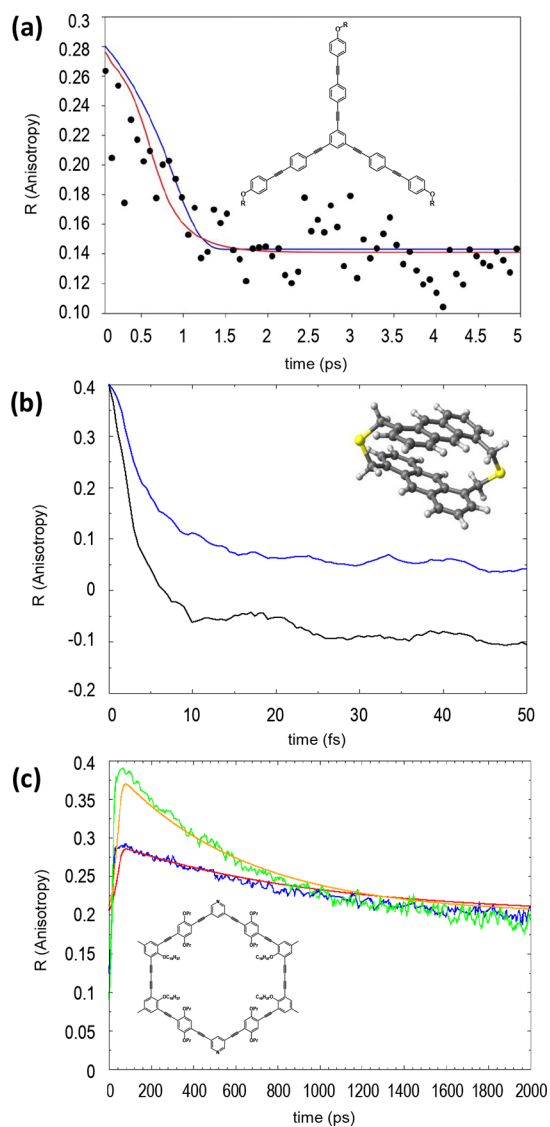


**Figure 5.** Examples of fluorescence anisotropy curves. (a) Simulated anisotropy decay curves for the linear PE dendrimer (blue) compared with experimental data (black) (fitting in red). (b) Simulated anisotropy decay for a single dimethyl anthracene (DMA) chromophore (blue) compared to the dithia-anthracenophane (DTA) dimer (black). (c) Simulated anisotropy decay for the PE macrocycle (red) and the half ring (orange) compared with experimental data (blue and green, respectively).

the macrocycle results from the interference of several  
628 pathways. 629

*Concluding Remarks.* The coupling between electronic and  
630 nuclear motions defined by nonadiabatic dynamics character-  
631 izes the formation, evolution, and decay of excitations in  
632 photoactive materials. The modeling of such complex dynamics  
633 can be achieved with semiclassical surface hopping-based  
634 approaches to go beyond the Born–Oppenheimer approx-  
635 imation. Sophisticated atomistic modeling in the subnano-  
636 second regime allows information such as absorption and  
637 emission spectra, relaxation time scales, and excited state  
638 lifetimes to be accurately predicted but also reveals more  
639 complicated exciton migration pathways and mechanisms. Such  
640 simulations can provide intricate details into the vibrational  
641 motions driving the concomitant electronic transitions that  
642 ultimately lead to changes in localization associated with energy 643



644 transfer. Within the nonadiabatic excited state molecular  
645 dynamics formulation, the transition density matrices describe  
646 the photoinduced spatial changes in localization that accom-  
647 pany energy transfer allowing multichromophore systems to be  
648 partitioned into contributions from individual fragments. The  
649 changes in localization are directly coupled to high-frequency  
650 nuclear motions that drive the nonadiabatic transitions. Specific  
651 motions involving bond lengths and torsion angles can be  
652 enhanced by strain to break conjugation and promote  
653 electronic energy redistribution and exciton trapping.

654 Conformational sampling diversity, which is strongly  
655 influenced by thermal fluctuations to produce a variety of  
656 initial conditions, affect the electronic transition density  
657 localization and available energy transfer pathways. Nuclear  
658 motions along polymer or dendrimer backbones can cause  
659 kinks that break conjugation and/or bring excited states  
660 localized on different chromophore units into resonance  
661 allowing ultrafast flow of energy between them. This disorder  
662 makes it almost impossible to apply the Förster model, which  
663 cannot adequately describe multiple complex rates caused by  
664 energy reordering and interference among competing pathways.  
665 Furthermore, the presence of identical chromophores makes it  
666 difficult to distinguish between possible mechanisms that result  
667 in the spatial scrambling of the transition dipole orientation. In  
668 such cases, the ambiguity can be overcome by choosing the  
669 assignment of chromophore fragments based on the initial or  
670 final localization or through the statistical minimum flow  
671 method to track energy flow between units.

672 The effects we have demonstrated here relate to long-lived  
673 coherence phenomena observed in multiple materials via  
674 sophisticated spectroscopies.<sup>106</sup> Here, they clearly result from  
675 a vibrational signature modulating the electronic states and  
676 bringing them into resonance. We suggest that focusing the  
677 attention on the specific role vibrational dynamics plays in  
678 guiding electronic dynamics can provide a deeper under-  
679 standing of existing problems in photochemistry, photobiology,  
680 and the tailor design of photoactive materials. The insights  
681 gained from modeling will provide new interpretations of  
682 experimental measurements, such as fluorescence anisotropy  
683 decay and transient absorption spectroscopy, based on the  
684 particular combination of photophysical processes and  
685 competing mechanisms.

## 686 ■ AUTHOR INFORMATION

### 687 Corresponding Author

688 \*E-mail: [serg@lanl.gov](mailto:serg@lanl.gov).

### 689 ORCID

690 Tammie Nelson: 0000-0002-3173-5291

691 Adrian E. Roitberg: 0000-0003-3963-8784

692 Sergei Tretiak: 0000-0001-5547-3647

### 693 Notes

694 The authors declare no competing financial interest.

### 695 Biographies

696 **Dr. Tammie Nelson** is a Staff Scientist at Los Alamos National  
697 Laboratory. She received her undergraduate degree from California  
698 Polytechnic State University (San Luis Obispo) in 2008 and her Ph.D.  
699 (2013) in Chemistry from the University of Rochester, NY. Her  
700 research interests include the development of efficient methods for  
701 modeling photoinduced processes in realistic molecular systems and  
702 the application of nonadiabatic excited state molecular dynamics to  
703 photochemistry in nanomaterials.

**Dr. Sebastian Fernandez Alberti** is a Full Professor at National  
704 University of Quilmes (UNQ, Argentina) and Independent Researcher  
705 at the National Council for Scientific and Technical Research  
706 (CONICET, Argentina). He received his undergraduate degree in  
707 1993 from the National University of La Plata (UNLP, Argentina) and  
708 his Ph.D. in Molecular Physics in 1999 from the University of Paul  
709 Sabatier (Toulouse, France). His research interests include excited-  
710 state nonadiabatic dynamics simulations in extended conjugated  
711 molecules, electronic and vibrational relaxation, intramolecular energy  
712 redistribution in polyatomic molecules, and protein dynamics analysis  
713 using collective coordinates. 714

**Dr. Adrian E. Roitberg** is a Full Professor in the Chemistry  
715 Department at the University of Florida. He received his under-  
716 graduate degree from the University of Buenos Aires, Argentina, in  
717 1987, and his Ph.D. from the University of Illinois at Chicago in 1992.  
718 He joined the University of Florida in 2001. His research interests are  
719 molecular modeling of molecules and materials, and studying the effect  
720 of dynamics and conformational diversity of experimental observables. 721

**Dr. Sergei Tretiak** is a Staff Scientist at Los Alamos National  
722 Laboratory. He received his M.Sc. degree from Moscow Institute of  
723 Physics and Technology (Russia) and his Ph.D. degree in 1998 from  
724 the University of Rochester. Since 2006 Tretiak has been a member of  
725 the DOE funded Center for Integrated Nanotechnologies (CINT). He  
726 also serves as an Adjunct Professor at the University of California,  
727 Santa Barbara (2015–present) and at Skolkovo Institute of Science  
728 and Technology, Moscow, Russia (2013–present). His research  
729 interests include development of modern computational methods for  
730 molecular optical properties, nonlinear optical response of organic  
731 chromophores, adiabatic and nonadiabatic molecular dynamics of  
732 excited states, optical response of confined excitons in conjugated  
733 polymers, carbon nanotubes, semiconductor nanoparticles, halide  
734 perovskites, and molecular aggregates. 735

## 736 ■ ACKNOWLEDGMENTS

S.F.A. is supported by CONICET, UNQ, ANPCyT (PICT-  
737 2014-2662). S.T. and T.N. acknowledge support from Los  
738 Alamos National Laboratory (LANL) Directed Research and  
739 Development Funds (LDRD). This research used resources  
740 provided by the Los Alamos National Laboratory Institutional  
741 Computing (IC) Program, which is supported by the U.S.  
742 Department of Energy National Nuclear Security Adminis-  
743 tration. Los Alamos National Laboratory is operated by Los  
744 Alamos National Security, LLC, for the National Nuclear  
745 Security Administration of the U.S. Department of Energy  
746 under contract DE-AC52-06NA25396. We acknowledge  
747 support of the Center for Integrated Nanotechnology  
748 (CINT), a U.S. Department of Energy, Office of Basic Energy  
749 Sciences user facility. 750

## 751 ■ REFERENCES

- 752 (1) Fidler, A. F.; Singh, V. P.; Long, P. D.; Dahlberg, P. D.; Engel, G.  
753 S. Dynamic Localization of Electronic Excitations in Photosynthetic  
754 Complexes Revealed with Chiral Two-Dimensional Spectroscopy. *Nat.*  
755 *Commun.* **2014**, *5*, 3286.
- 756 (2) Scholes, G. D.; Fleming, G. R. On the Mechanism of Light  
757 Harvesting in Photosynthetic Purple Bacteria: B800 to B850 Energy  
758 Transfer. *J. Phys. Chem. B* **2000**, *104*, 1854–1868.
- 759 (3) Lefler, K. M.; Kim, C. H.; Wu, Y. L.; Wasielewski, M. R. Self-  
760 Assembly of Supramolecular Light-Harvesting Arrays from Symmetric  
761 Perylene-3,4-dicarboximide Trefolds. *J. Phys. Chem. Lett.* **2014**, *5*,  
762 1608–1615.

- 763 (4) Uetomo, A.; Kozaki, M.; Suzuki, S.; Yamanaka, K.; Ito, O.;  
764 Okada, K. Efficient Light-Harvesting Antenna with a Multi-Porphyrin  
765 Cascade. *J. Am. Chem. Soc.* **2011**, *133*, 13276–13279.
- 766 (5) Leishman, C. W.; McHale, J. L. Light-Harvesting Properties and  
767 Morphology of Porphyrin Nanostructures Depend on Ionic Species  
768 Inducing Aggregation. *J. Phys. Chem. C* **2015**, *119*, 28167–28181.
- 769 (6) Ishida, Y.; Shimada, T.; Masui, D.; Tachibana, H.; Inoue, H.;  
770 Takagi, S. Efficient Excited Energy Transfer Reaction in Clay/  
771 Porphyrin Complex Toward an Artificial Light-Harvesting System. *J.*  
772 *Am. Chem. Soc.* **2011**, *133*, 14280–14286.
- 773 (7) Ziessel, R.; Ulrich, G.; Haefele, A.; Harriman, A. An Artificial  
774 Light-Harvesting Array Constructed from Multiple Bodipy Dyes. *J.*  
775 *Am. Chem. Soc.* **2013**, *135*, 11330–11344.
- 776 (8) Lee, C. Y.; Farha, O. K.; Hong, B. J.; Sarjeant, A. A.; Nguyen, S.  
777 T.; Hupp, J. T. Light-Harvesting Metal-Organic Frameworks (MOFs):  
778 Efficient Strut-to-Strut Energy Transfer in Bodipy and Porphyrin-  
779 Based MOFs. *J. Am. Chem. Soc.* **2011**, *133*, 15858–15861.
- 780 (9) Johnson, J. M.; Chen, R.; Chen, X.; Moskun, A. C.; Zhang, X.;  
781 Hogen-Esch, T. E.; Bradforth, S. E. Investigation of Macrocyclic  
782 Polymers as Artificial Light Harvesters: Subpicosecond Energy  
783 Transfer in Poly(9,9-Dimethyl-2-Vinylfluorene). *J. Phys. Chem. B*  
784 **2008**, *112*, 16367–16381.
- 785 (10) Aggarwal, A. V.; Thiessen, A.; Idelson, A.; Kalle, D.; Würsch, D.;  
786 Stangl, T.; Steiner, F.; Jester, S.-S.; Vogelsang, J.; Höger, S.; et al.  
787 Fluctuating Exciton Localization in Giant  $\pi$ -Conjugated Spoked-Wheel  
788 Macrocycles. *Nat. Chem.* **2013**, *5*, 964–970.
- 789 (11) Swallen, S. F.; Kopelman, R.; Moore, J. S.; Devadoss, C.  
790 Dendrimer Photoantenna Supermolecules: Energetic Funnels, Exciton  
791 Hopping and Correlated Excimer Formation. *J. Mol. Struct.* **1999**,  
792 *485–486*, 585–597.
- 793 (12) Andrews, D. L. Light Harvesting in Dendrimer Materials:  
794 Designer Photophysics and Electrodynamics. *J. Mater. Res.* **2012**, *27*,  
795 627–638.
- 796 (13) Bradshaw, D. S.; Andrews, D. L. Mechanisms of Light Energy  
797 Harvesting in Dendrimers and Hyperbranched Polymers. *Polymers*  
798 **2011**, *3*, 2053–2077.
- 799 (14) Bosman, A. W.; Janssen, H. M.; Meijer, E. W. About  
800 Dendrimers: Structure, Physical Properties, and Applications. *Chem.*  
801 *Rev.* **1999**, *99*, 1665–1688.
- 802 (15) Ostroumov, E. E.; Mulvaney, R. M.; Cogdell, R. J.; Scholes, G.  
803 D. Broadband 2D Electronic Spectroscopy Reveals a Carotenoid Dark  
804 State in Purple Bacteria. *Science* **2013**, *340*, 52–56.
- 805 (16) Bakulin, A. A.; Silva, C.; Vella, E. Ultrafast Spectroscopy with  
806 Photocurrent Detection: Watching Excitonic Optoelectronic Systems  
807 at Work. *J. Phys. Chem. Lett.* **2016**, *7*, 250–258.
- 808 (17) Soavi, G.; Scotognella, F.; Lanzani, G.; Cerullo, G. Ultrafast  
809 Photophysics of Single-Walled Carbon Nanotubes. *Adv. Opt. Mater.*  
810 **2016**, *4*, 1670–1688.
- 811 (18) Galindo, J. F.; Atas, E.; Altan, A.; Kuroda, D. G.; Fernandez-  
812 Alberti, S.; Tretiak, S.; Roitberg, A. E.; Kleiman, V. D. Dynamics of  
813 Energy Transfer in a Conjugated Dendrimer Driven by Ultrafast  
814 Localization of Excitations. *J. Am. Chem. Soc.* **2015**, *137*, 11637–  
815 11644.
- 816 (19) Bradforth, S. E.; Jimenez, R.; van Mourik, F.; van Grondelle, R.;  
817 Fleming, G. R. Excitation Transfer in the Core Light-Harvesting  
818 Complex (LH-1) of Rhodospirillum rubrum: An Ultrafast  
819 Fluorescence Depolarization and Annihilation Study. *J. Phys. Chem.*  
820 **1995**, *99*, 16179–16191.
- 821 (20) Camacho, R.; Tubasum, S.; Southall, J.; Cogdell, R. J.;  
822 Sforzini, G.; Anderson, H. L.; Pullerits, T.; Scheblykin, I. G.  
823 Fluorescence Polarization Measures Energy Funneling in Single Light-  
824 Harvesting Antennas - LH2 vs Conjugated Polymers. *Sci. Rep.* **2015**, *5*,  
825 15080.
- 826 (21) Yong, C.-K.; Parkinson, P.; Kondratuk, D.; Chen, W.-H.;  
827 Stannard, A.; Summerfield, A.; Sprafke, J.; O'Sullivan, M.; Beton, P.;  
828 Anderson, H.; et al. Ultrafast Delocalization of Excitation in Synthetic  
829 Light-Harvesting Nanorings. *Chem. Sci.* **2015**, *6*, 181–189.
- 830 (22) Varnavski, O.; Samuel, I. D. W.; Palsson, L.-O.; Beavington, R.;  
831 Burn, P. L.; Goodson, T. Investigations of Excitation Energy Transfer  
and Intramolecular Interactions in a Nitrogen Corded Distyrylbenzene  
Dendrimer System. *J. Chem. Phys.* **2002**, *116*, 8893.
- (23) Schmid, S. A.; Yim, K. H.; Chang, M. H.; Zheng, Z.; Huck, W.  
T. S.; Friend, R. H.; Kim, J. S.; Herz, L. M. Polarization Anisotropy  
Dynamics for Thin Films of a Conjugated Polymer Aligned by  
Nanoimprinting. *Phys. Rev. B: Condens. Matter Mater. Phys.* **2008**, *77*,  
115338.
- (24) Dykstra, T. E.; Hennebicq, E.; Beljonne, D.; Gierschner, J.;  
Claudio, G.; Bittner, E. R.; Knoester, J.; Scholes, G. D. Conformational  
Disorder and Ultrafast Exciton Relaxation in PPV-family Conjugated  
Polymers. *J. Phys. Chem. B* **2009**, *113*, 656–667.
- (25) Yamazaki, I.; Akimoto, S.; Yamazaki, T.; Sato, S.-I.; Sakata, Y.  
Oscillatory Exciton Transfer in Dithiaanthracenophane: Quantum  
Beat a Coherent Photochemical Process in Solution. *J. Phys. Chem. A*  
**2002**, *106*, 2122–2128.
- (26) Zhu, F.; Galli, C.; Hochstrasser, R. M. The Real-Time  
Intramolecular Electronic Excitation Transfer Dynamics of 9',9'-  
Bifluorene and 2',2'-Binaphthyl in Solution. *J. Chem. Phys.* **1993**, *98*,  
1042–1057.
- (27) Newbloom, G. M.; Hoffmann, S. M.; West, A. F.; Gile, M. C.;  
Sista, P.; Cheung, H.-K. C.; Luscombe, C. K.; Pfaendtner, J.; Pozzo, L.  
D. Solvatochromism and Conformational Changes in Fully Dissolved  
Poly(3-Alkylthiophene)s. *Langmuir* **2015**, *31*, 458–468.
- (28) Petrone, A.; Goings, J. J.; Li, X. Quantum Confinement Effects  
on Optical Transitions in Nanodiamonds Containing Nitrogen  
Vacancies. *Phys. Rev. B: Condens. Matter Mater. Phys.* **2016**, *94*, 165402.
- (29) Müller, J. G.; Atas, E.; Tan, C.; Schanze, K. S.; Kleiman, V. D.  
The Role of Exciton Hopping and Direct Energy Transfer in the  
Efficient Quenching of Conjugated Polyelectrolytes. *J. Am. Chem. Soc.*  
**2006**, *128*, 4007–4016.
- (30) Ikeda, T.; Lee, B.; Kurihara, S.; Tazuke, S.; Ito, S.; Yamamoto,  
M. Time-Resolved Observation of Excitation Hopping Between Two  
Identical Chromophores Attached to Both Ends of Alkanes. *J. Am.*  
*Chem. Soc.* **1988**, *110*, 8299–8304.
- (31) Hestand, N. J.; Spano, F. C. The Effect of Chain Bending on the  
Photophysical Properties of Conjugated Polymers. *J. Phys. Chem. B*  
**2014**, *118*, 8352–8363.
- (32) Nayyar, I. H.; Batista, E. R.; Tretiak, S.; Saxena, A.; Smith, D. L.;  
Martin, R. L. Role of Geometric Distortion and Polarization in  
Localizing Electronic Excitations in Conjugated Polymers. *J. Chem.*  
*Theory Comput.* **2013**, *9*, 1144–1154.
- (33) Shi, T.; Li, H.; Tretiak, S.; Chernyak, V. Y. How Geometric  
Distortions Scatter Electronic Excitations in Conjugated Macro-  
molecules. *J. Phys. Chem. Lett.* **2014**, *5*, 3946–3952.
- (34) Becker, K.; Da Como, E.; Feldmann, J.; Scheliga, F.; Csanyi, E.;  
Tretiak, S.; Lupton, J. M. How Chromophore Shape Determines the  
Spectroscopy of Phenylene Vinylenes: Origin of Spectral Broadening  
in the Absence of Aggregation. *J. Phys. Chem. B* **2008**, *112*, 4859–  
4864.
- (35) Van Averbeke, B.; Beljonne, D. Conformational Effects on  
Excitation Transport Along Conjugated Polymer Chains. *J. Phys.*  
*Chem. A* **2009**, *113*, 2677–2682.
- (36) Nelson, T.; Fernandez-Alberti, S.; Roitberg, A. E.; Tretiak, S.  
Conformational Disorder in Energy Transfer: Beyond Förster Theory.  
*Phys. Chem. Chem. Phys.* **2013**, *15*, 9245–9256.
- (37) Ondarse-Alvarez, D.; Komurlu, S.; Roitberg, A. E.; Pierdominici-  
Sottile, G.; Tretiak, S.; Fernandez-Alberti, S.; Kleiman, V. D. Ultrafast  
Electronic Energy Relaxation in a Conjugated Dendrimer Leading to  
Inter-Branch Energy Redistribution. *Phys. Chem. Chem. Phys.* **2016**, *18*,  
25080–25089.
- (38) Ondarse-Alvarez, D.; Oldani, N.; Tretiak, S.; Fernandez-Alberti,  
S. Computational Study of Photoexcited Dynamics in Bichromophoric  
Cross-Shaped Oligofluorene. *J. Phys. Chem. A* **2014**, *118*, 10742–  
10753.
- (39) Nguyen, T.-Q.; Martini, I. B.; Liu, J.; Schwartz, B. J. Controlling  
Interchain Interactions in Conjugated Polymers: The Effects of Chain  
Morphology on Exciton-Exciton Annihilation and Aggregation in  
MEH-PPV Films. *J. Phys. Chem. B* **2000**, *104*, 237–255.

- 900 (40) Barbatti, M. Nonadiabatic Dynamics with Trajectory Surface  
901 Hopping Method. *Wiley Interdiscip. Rev. Comput. Mol. Sci.* **2011**, *1*,  
902 620–633.
- 903 (41) Wang, L.; Akimov, A.; Prezhdo, O. V. Recent Progress in  
904 Surface Hopping: 2011–2015. *J. Phys. Chem. Lett.* **2016**, *7*, 2100–  
905 2112.
- 906 (42) White, A.; Tretiak, S.; Mozyrsky, D. Coupled Wave-Packets for  
907 Non-Adiabatic Molecular Dynamics: A Generalization of Gaussian  
908 Wave-Packet Dynamics to Multiple Potential Energy Surfaces. *Chem.*  
909 *Sci.* **2016**, *7*, 4905–4911.
- 910 (43) Subotnik, J. E.; Jain, A.; Landry, B.; Petit, A.; Ouyang, W.;  
911 Bellonzi, N. Understanding the Surface Hopping View of Electronic  
912 Transitions and Decoherence. *Annu. Rev. Phys. Chem.* **2016**, *67*, 387–  
913 417.
- 914 (44) Zhu, C.; Nangia, S.; Jasper, A. W.; Truhlar, D. G. Coherent  
915 Switching with Decay of Mixing: An Improved Treatment of  
916 Electronic Coherence for Non-Born Oppenheimer Trajectories. *J.*  
917 *Chem. Phys.* **2004**, *121*, 7658–7670.
- 918 (45) Martens, C. C. Surface Hopping by Consensus. *J. Phys. Chem.*  
919 *Lett.* **2016**, *7*, 2610–2615.
- 920 (46) Richter, M.; Marquetand, P.; González-Vázquez, J.; Sola, I.;  
921 González, L. SHARC: ab Initio Molecular Dynamics with Surface  
922 Hopping in the Adiabatic Representation Including Arbitrary  
923 Couplings. *J. Chem. Theory Comput.* **2011**, *7*, 1253–1258.
- 924 (47) Granucci, G.; Persico, M.; Spighi, G. Surface Hopping  
925 Trajectory Simulations with Spin-Orbit and Dynamical Couplings. *J.*  
926 *Chem. Phys.* **2012**, *137*, 22A501.
- 927 (48) Cui, G.; Thiel, W. Generalized Trajectory Surface-Hopping  
928 Method for Internal Conversion and Intersystem Crossing. *J. Chem.*  
929 *Phys.* **2014**, *141*, 124101.
- 930 (49) Barbatti, M.; Ruckebauer, M.; Plasser, F.; Pittner, J.; Granucci,  
931 G.; Persico, M.; Lischka, H. Newton-X: A Surface-Hopping Program  
932 for Nonadiabatic Molecular Dynamics. *Wiley Interdiscip. Rev. Comput.*  
933 *Mol. Sci.* **2014**, *4*, 26–33.
- 934 (50) Churcho, B. F. E.; Rauer, C.; Marquetand, P.; González, L.;  
935 Martínez, T. J. Communication: GAIMS—Generalized Ab Initio  
936 Multiple Spawning for Both Internal Conversion and Intersystem  
937 Crossing Processes. *J. Chem. Phys.* **2016**, *144*, 101102.
- 938 (51) Ishida, T.; Nanbu, S.; Nakamura, H. Clarification of Non-  
939 adiabatic Chemical Dynamics by the Zhu-Nakamura Theory of  
940 Nonadiabatic Transition: From Tri-Atomic Systems to Reactions in  
941 Solutions. *Int. Rev. Phys. Chem.* **2017**, *36*, 229–286.
- 942 (52) Tully, J. Molecular Dynamics with Electronic Transitions. *J.*  
943 *Chem. Phys.* **1990**, *93*, 1061–1071.
- 944 (53) Soler, M. A.; Roitberg, A. E.; Nelson, T.; Tretiak, S.; Fernandez-  
945 Alberti, S. Analysis of State-Specific Vibrations Coupled to the  
946 Unidirectional Energy Transfer in Conjugated Dendrimers. *J. Phys.*  
947 *Chem. A* **2012**, *116*, 9802–9810.
- 948 (54) Soler, M. A.; Nelson, T.; Roitberg, A. E.; Tretiak, S.; Fernandez-  
949 Alberti, S. Signature of Nonadiabatic Coupling in Excited-State  
950 Vibrational Modes. *J. Phys. Chem. A* **2014**, *118*, 10372–10379.
- 951 (55) Shenai, P. M.; Fernandez-Alberti, S.; Bricker, W. P.; Tretiak, S.;  
952 Zhao, Y. Internal Conversion and Vibrational Energy Redistribution in  
953 Chlorophyll A. *J. Phys. Chem. B* **2016**, *120*, 49–58.
- 954 (56) Paterlini, M.; Ferguson, D. Constant Temperature Simulations  
955 using the Langevin Equation with Velocity Verlet Integration. *Chem.*  
956 *Phys.* **1998**, *236*, 243–252.
- 957 (57) Attard, P. Statistical Mechanical Theory for Non-Equilibrium  
958 Systems. IX. Stochastic Molecular Dynamics. *J. Chem. Phys.* **2009**, *130*,  
959 194113.
- 960 (58) Tretiak, S.; Chernyak, V.; Mukamel, S. Two-Dimensional Real-  
961 Space Analysis of Optical Excitations in Acceptor-Substituted  
962 Carotenoids. *J. Am. Chem. Soc.* **1997**, *119*, 11408–11419.
- 963 (59) Tretiak, S.; Chernyak, V.; Mukamel, S. Collective Electronic  
964 Oscillators for Nonlinear Optical Response of Conjugated Molecules.  
965 *Chem. Phys. Lett.* **1996**, *259*, 55–61.
- 966 (60) Stewart, J. J. P. Optimization of Parameters for Semiempirical  
967 Methods. I. Method. *J. Comput. Chem.* **1989**, *10*, 209–220.
- (61) Stewart, J. J. P. Optimization of Parameters for Semiempirical  
Methods. II. Applications. *J. Comput. Chem.* **1989**, *10*, 221–264. 968
- (62) Hernandez, L. A.; Nelson, T.; Tretiak, S.; Fernandez-Alberti, S. 969  
Photoexcited Energy Transfer in a Weakly Coupled Dimer. *J. Phys.*  
*Chem. B* **2015**, *119*, 7242–7252. 970–972
- (63) Alfonso Hernandez, L.; Nelson, T.; Gelin, M. F.; Lupton, J. M.; 973  
Tretiak, S.; Fernandez-Alberti, S. Interference of Interchromophoric  
Energy-Transfer Pathways in  $\pi$ -Conjugated Macrocycles. *J. Phys.*  
*Chem. Lett.* **2016**, *7*, 4936–4944. 974–976
- (64) Nelson, T.; Fernandez-Alberti, S.; Chernyak, V.; Roitberg, A. E.; 977  
Tretiak, S. Nonadiabatic Excited-State Molecular Dynamics Modeling  
of Photoinduced Dynamics in Conjugated Molecules. *J. Phys. Chem. B* 978  
**2011**, *115*, 5402–5414. 979–980
- (65) Nelson, T.; Fernandez-Alberti, S.; Chernyak, V.; Roitberg, A.; 981  
Tretiak, S. Nonadiabatic Excited-State Molecular Dynamics: Numerical  
Tests of Convergence and Parameters. *J. Chem. Phys.* **2012**, *136*, 982  
054108. 983–984
- (66) Fernandez-Alberti, S.; Roitberg, A.; Nelson, T.; Tretiak, S. 985  
Identification of Unavoided Crossings in Nonadiabatic Photoexcited  
Dynamics Involving Multiple Electronic States in Polyatomic  
Conjugated Molecules. *J. Chem. Phys.* **2012**, *137*, 014512. 986–988
- (67) Nelson, T.; Fernandez-Alberti, S.; Roitberg, A. E.; Tretiak, S. 989  
Nonadiabatic Excited-State Molecular Dynamics: Treatment of  
Electronic Decoherence. *J. Chem. Phys.* **2013**, *138*, 224111. 990–991
- (68) Nelson, T.; Fernandez-Alberti, S.; Roitberg, A. E.; Tretiak, S. 992  
Nonadiabatic Excited-State Molecular Dynamics: Modeling Photo-  
physics in Organic Conjugated Materials. *Acc. Chem. Res.* **2014**, *47*, 993  
1155–1164. 994–995
- (69) Fernandez-Alberti, S.; Roitberg, A. E.; Kleiman, V. D.; Nelson, 996  
T.; Tretiak, S. Shishiodoshi Unidirectional Energy Transfer Mecha-  
nism in Phenylene Ethynylene Dendrimers. *J. Chem. Phys.* **2012**, *137*, 997  
22A526. 998–999
- (70) Franklin-Mergarejo, R.; Alvarez, D. O.; Tretiak, S.; Fernandez- 1000  
Alberti, S. Carbon Nanorings with Inserted Acenes: Breaking  
Symmetry in Excited State Dynamics. *Sci. Rep.* **2016**, *6*, 31253. 1001–1002
- (71) Bricker, W. P.; Shenai, P. M.; Ghosh, A.; Liu, Z.; Grace, M.; 1003  
Enriquez, M.; Lambrev, P. H.; Tan, H.-S.; Lo, C. S.; Tretiak, S.; et al.  
Non-radiative Relaxation of Photoexcited Chlorophylls: Theoretical  
and Experimental Study. *Sci. Rep.* **2015**, *5*, 13625. 1004–1006
- (72) Clark, J.; Nelson, T.; Tretiak, S.; Cirmi, G.; Lanzani, G. 1007  
Femtosecond Torsional Relaxation. *Nat. Phys.* **2012**, *8*, 225–231. 1008
- (73) Nelson, T.; Naumov, A.; Fernandez-Alberti, S.; Tretiak, S. 1009  
Nonadiabatic Excited-State Molecular Dynamics: On-the-fly Limiting  
of Essential Excited States. *Chem. Phys.* **2016**, *481*, 84–90. 1010–1011
- (74) Nelson, T.; Fernandez-Alberti, S.; Roitberg, A. E.; Tretiak, S. 1012  
Artifacts Due to Trivial Unavoided Crossings in the Modeling of  
Photoinduced Energy Transfer Dynamics in Extended Conjugated  
Molecules. *Chem. Phys. Lett.* **2013**, *590*, 208–213. 1013–1015
- (75) Wang, L.; Prezhdo, O. V. A Simple Solution to the Trivial 1016  
Crossing Problem in Surface Hopping. *J. Phys. Chem. Lett.* **2014**, *5*,  
713–719. 1017–1018
- (76) Meek, G. A.; Levine, B. G. Evaluation of the Time-Derivative 1019  
Coupling for Accurate Electronic State Transition Probabilities from  
Numerical Simulations. *J. Phys. Chem. Lett.* **2014**, *5*, 2351–2356. 1020–1021
- (77) Jain, A.; Alguire, E.; Subotnik, J. E. An Efficient, Augmented 1022  
Surface Hopping Algorithm that Includes Decoherence for Use in  
Large-Scale Simulations. *J. Chem. Theory Comput.* **2016**, *12*, 5256–  
5268. 1023–1025
- (78) Jaeger, H. M.; Fischer, S.; Prezhdo, O. V. Decoherence-Induced 1026  
Surface Hopping. *J. Chem. Phys.* **2012**, *137*, 22A545. 1027
- (79) Granucci, G.; Persico, M.; Zocante, A. Including Quantum 1028  
Decoherence in Surface Hopping. *J. Chem. Phys.* **2010**, *133*, 134111. 1029
- (80) Subotnik, J. E. Fewest-Switches Surface Hopping and 1030  
Decoherence in Multiple Dimensions. *J. Phys. Chem. A* **2011**, *115*,  
12083–12096. 1031–1032
- (81) Herman, M. F. Toward an Accurate and Efficient Semiclassical 1033  
Surface Hopping Procedure for Nonadiabatic Problems. *J. Phys. Chem.*  
*A* **2005**, *109*, 9196–9205. 1034–1035

- (82) Miller, W. H. The Semiclassical Initial Value Representation: A Potentially Practical Way for Adding Quantum Effects to Classical Molecular Dynamics Simulations. *J. Phys. Chem. A* **2001**, *105*, 2942–2955.
- (83) Miller, W. H. Electronically Nonadiabatic Dynamics via Semiclassical Initial Value Methods. *J. Phys. Chem. A* **2009**, *113*, 1405–1415.
- (84) Ben-Nun, M.; Quenneville, J.; Martínez, T. J. Ab Initio Multiple Spawning: Photochemistry from First Principles Quantum Molecular Dynamics. *J. Phys. Chem. A* **2000**, *104*, S161–S175.
- (85) White, A. J.; Gorshkov, V. N.; Wang, R.; Tretiak, S.; Mozysky, D. Semiclassical Monte Carlo: A First Principles Approach to Non-Adiabatic Molecular Dynamics. *J. Chem. Phys.* **2014**, *141*, 184101.
- (86) Kong, X.; Markmann, A.; Batista, V. S. Time-Sliced Thawed Gaussian Propagation Method for Simulations of Quantum Dynamics. *J. Phys. Chem. A* **2016**, *120*, 3260–3269.
- (87) Tretiak, S.; Mukamel, S. Density Matrix Analysis and Simulation of Electronic Excitations in Conjugated and Aggregated Molecules. *Chem. Rev.* **2002**, *102*, 3171–3212.
- (88) Mukamel, S.; Tretiak, S.; Wagersreiter, T.; Chernyak, V. Electronic Coherence and Collective Optical Excitations of Conjugated Molecules. *Science* **1997**, *277*, 781–787.
- (89) Martin, R. L. Natural Transition Orbitals. *J. Chem. Phys.* **2003**, *118*, 4775–4777.
- (90) Tretiak, S.; Isborn, C.; Niklasson, A.; Challacombe, M. Representation Independent Algorithms for Molecular Response Calculations in Time-Dependent Self-Consistent Field Theories. *J. Chem. Phys.* **2009**, *130*, 054111.
- (91) Karabunarliev, S.; Baumgarten, M.; Bittner, E. R.; Mullen, K. Rigorous Franck Condon Absorption and Emission Spectra of Conjugated Oligomers from Quantum Chemistry. *J. Chem. Phys.* **2000**, *113*, 11372–11381.
- (92) Gong, J. Q.; Favereau, L.; Anderson, H. L.; Herz, L. M. Breaking the Symmetry in Molecular Nanorings. *J. Phys. Chem. Lett.* **2016**, *7*, 332–338.
- (93) Tommasini, M.; Chernyak, V.; Mukamel, S. Electronic Density-Matrix Algorithm for Nonadiabatic Couplings in Molecular Dynamics Simulations. *Int. J. Quantum Chem.* **2001**, *85*, 225–238.
- (94) Mathew, S.; Yella, A.; Gao, P.; Humphry-Baker, R.; Curchod, B. F. E.; Ashari-Astani, N.; Tavernelli, I.; Rothlisberger, U.; Nazeeruddin, M. K.; Grätzel, M. Dye-Sensitized Solar Cells with 13% Efficiency Achieved Through the Molecular Engineering of Porphyrin Sensitizers. *Nat. Chem.* **2014**, *6*, 242–247.
- (95) Landry, B. R.; Subotnik, J. E. Quantifying the Lifetime of Triplet Energy Transfer Processes in Organic Chromophores: A Case Study of 4-(2-Naphthylmethyl)Benzaldehyde. *J. Chem. Theory Comput.* **2014**, *10*, 4253–4263.
- (96) Jaegermann, P.; Plato, M.; von Maltzan, B.; Mobius, K. Time-Resolved EPR Study of Exciton Hopping in Porphyrin Dimers in Their Photoexcited Triplet State. *Mol. Phys.* **1993**, *78*, 1057–1074.
- (97) Tero-Kubota, S.; Miyamoto, T.; Akiyama, K.; Ikegami, Y.; Mataka, S.; Tashiro, M. Coherent and Incoherent Hopping of Triplet Exciton in Quinoxaline-Annulated and Naphthalene-Annulated Dimers. *Chem. Phys. Lett.* **1996**, *249*, 314–318.
- (98) Sung, J.; Kim, P.; Fimmel, B.; Wurthner, F.; Kim, D. Direct Observation of Ultrafast Coherent Exciton Dynamics in Helical  $\pi$ -Stacks of Self-Assembled Perylene Bisimides. *Nat. Commun.* **2015**, *6*, 8646.
- (99) Yang, L.; Caprasecca, S.; Mennucci, B.; Jang, S. Theoretical Investigation of the Mechanism and Dynamics of Intramolecular Coherent Resonance Energy Transfer in Soft Molecules: A Case Study of Dithia-anthracenophane. *J. Am. Chem. Soc.* **2010**, *132*, 16911–16921.
- (100) Sato, S.-I.; Nishimura, Y.; Sakata, Y.; Yamazaki, I. Coherent Control of Oscillatory Exciton Transfer in Dithia-1,5(3,3)-anthracenophane by a Phase-Locked Femtosecond Pulse Pair. *J. Phys. Chem. A* **2003**, *107*, 10019–10025.
- (101) Adamska, L.; Nayyar, I.; Chen, H.; Swan, A. K.; Oldani, N.; Fernandez-Alberti, S.; Golder, M. R.; Jasti, R.; Doorn, S. K.; Tretiak, S. Self-Trapping of Excitons, Violation of Condon Approximation, and Efficient Fluorescence in Conjugated Cycloparaphenylenes. *Nano Lett.* **2014**, *14*, 6539–6546.
- (102) Parkinson, P.; Kondratuk, D. V.; Menelaou, C.; Gong, J. Q.; Anderson, H. L.; Herz, L. M. Chromophores in Molecular Nanorings: When Is a Ring a Ring? *J. Phys. Chem. Lett.* **2014**, *5*, 4356–4361.
- (103) Darzi, E. R.; Hirst, E. S.; Weber, C. D.; Zakharov, L. N.; Lonergan, M. C.; Jasti, R. Synthesis, Properties, and Design Principles of Donor-Acceptor Nanohoops. *ACS Cent. Sci.* **2015**, *1*, 335–342.
- (104) Yousaf, M.; Lough, A. J.; Schott, E.; Koivisto, B. D. BODIPY-Phenylacetylene Macrocycle Motifs for Enhanced Light-Harvesting and Energy Transfer Applications. *RSC Adv.* **2015**, *5*, 57490–57492.
- (105) Kilina, S. V.; Kilin, D. S.; Prezhdo, O. V. Breaking the Phonon Bottleneck in PbSe and CdSe Quantum Dots: Time-Domain Density Functional Theory of Charge Carrier Relaxation. *ACS Nano* **2009**, *3*, 93–99.
- (106) Scholes, G. D.; Fleming, G. R.; Chen, L. X.; Aspuru-Guzik, A.; Buchleitner, A.; Coker, D. F.; Engel, G. S.; van Grondelle, R.; Ishizaki, A.; Jonas, D. M.; et al. Using Coherence to Enhance Function in Chemical and Biophysical Systems. *Nature* **2017**, *543*, 647–656.